nature materials

SUPPLEMENTARY INFORMATION

https://doi.org/10.1038/s41563-020-0713-9

In the format provided by the authors and unedited.

Gate-tunable spin waves in antiferromagnetic atomic bilayers

Xiao-Xiao Zhang[1,2], Lizhong Li[3], Daniel Weber[4], Joshua Goldberger[4], Kin Fai Mak[1,3,5] ✉ and Jie Shan[1,3,5] ✉

[1]Kavli Institute at Cornell for Nanoscale Science, Ithaca, NY, USA. [2]Department of Physics, University of Florida, Gainesville, FL, USA. [3]School of Applied and Engineering Physics, Cornell University, Ithaca, NY, USA. [4]Department of Chemistry and Biochemistry, Ohio State University, Columbus, OH, USA. [5]Laboratory of Atomic and Solid State Physics, Cornell University, Ithaca, NY, USA. ✉e-mail: kinfai.mak@cornell.edu; jie.shan@cornell.edu

Supplementary data and figures for
"Gate-tunable spin waves in antiferromagnetic atomic bilayers"

Xiao-Xiao Zhang, Lizhong Li, Daniel Weber, Joshua Goldberger, Kin Fai Mak, Jie Shan

[1]Kavli Institute at Cornell for Nanoscale Science, Ithaca, New York, USA
[2]Department of Physics, University of Florida, Gainesville, Florida, USA
[3]School of Applied and Engineering Physics, Cornell University, Ithaca, New York, USA
[4]Department of Chemistry and Biochemistry, Ohio State University, Columbus, Ohio, USA
[5]Laboratory of Atomic and Solid State Physics, Cornell University, Ithaca, New York, USA
Email: kinfai.mak@cornell.edu; jie.shan@cornell.edu

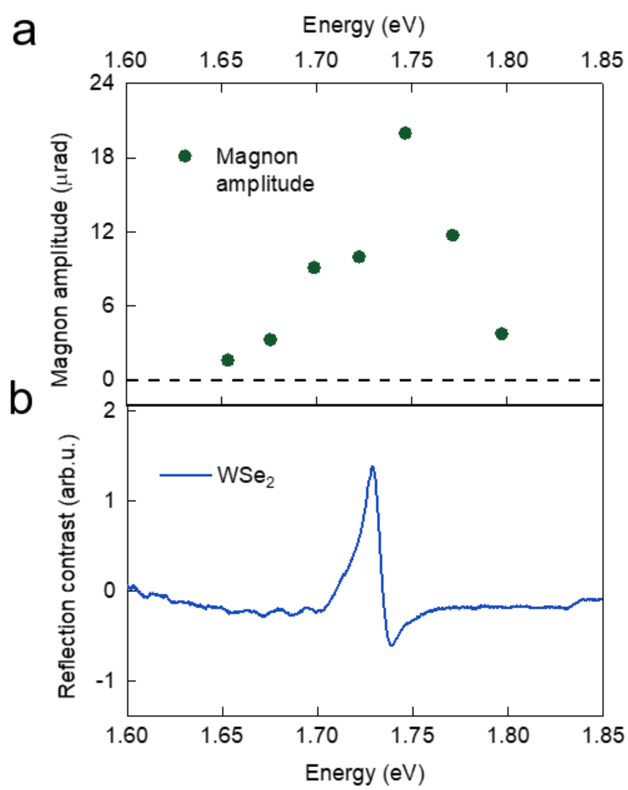

Figure S1 | Pump energy dependence of magnon amplitude. a, Amplitude of the high-energy spin waves under a fixed in-plane magnetic field of 2 T as a function of pump photon energy. **b,** Reflection contrast spectrum of WSe_2 on CrI_3. The spectrum is modified due to the local field factor in the device structure. The pump-energy dependence of the magnon amplitude resembles that of the excitonic resonance in monolayer WSe_2. The spectral broadening may arise from the additional WSe_2 trion absorption and bandwidth of the light pulses (~ 5 nm in full width at half maximum (FWHM)) employed in the pump-probe measurement.

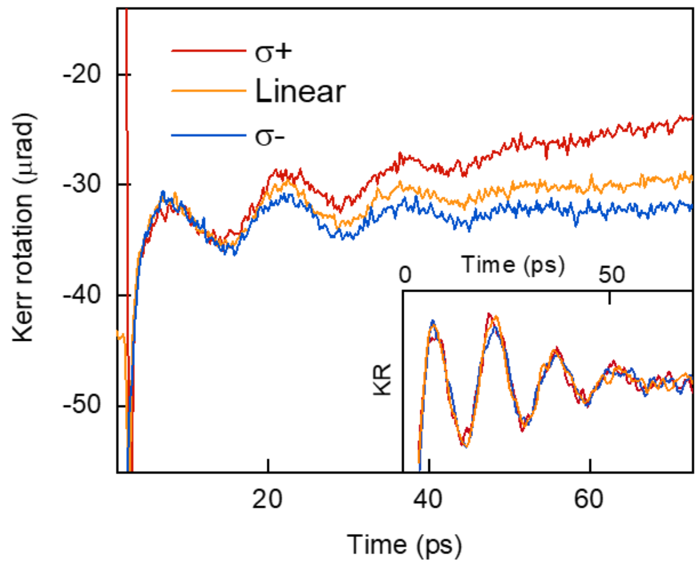

Figure S2 |Pump polarization dependence of the spin-wave dynamics. Time-resolved magnetic circular dichroism (MOKE) in bilayer CrI_3 under an in-plane field of 2 T excited by left circularly polarized (red), linear polarized (orange), and right circularly polarized pump (blue). The curves were vertically shifted for easy comparison. Inset: amplitude of the oscillations (after subtraction of the demagnetization dynamics) does not depend on the pump polarization (i.e. photon angular momentum).

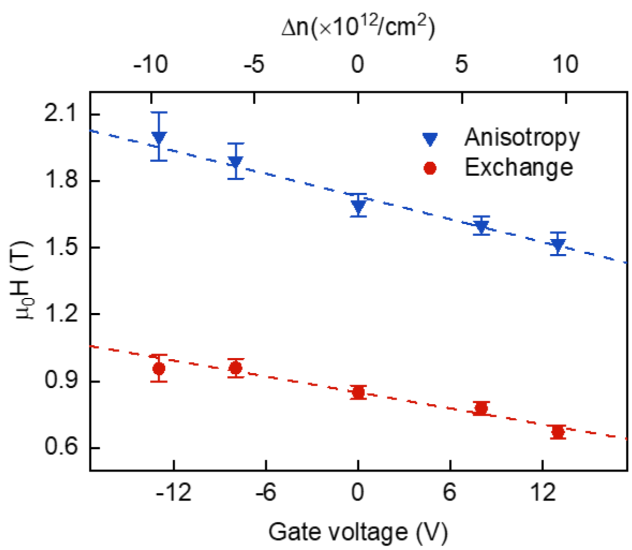

Figure S3| Gate-tunable magnetic interactions. Magnetic anisotropy (blue) and interlayer exchange fields (red) in bilayer CrI_3 as a function of gate voltage (bottom axis) and gate-induced doping density (top axis). Symbols are experiment. Error bars are the standard deviation from the Landau-Lifshitz-Gilbert (LLG) equation analysis shown in Fig. 4b. Dashed lines are linear fits.

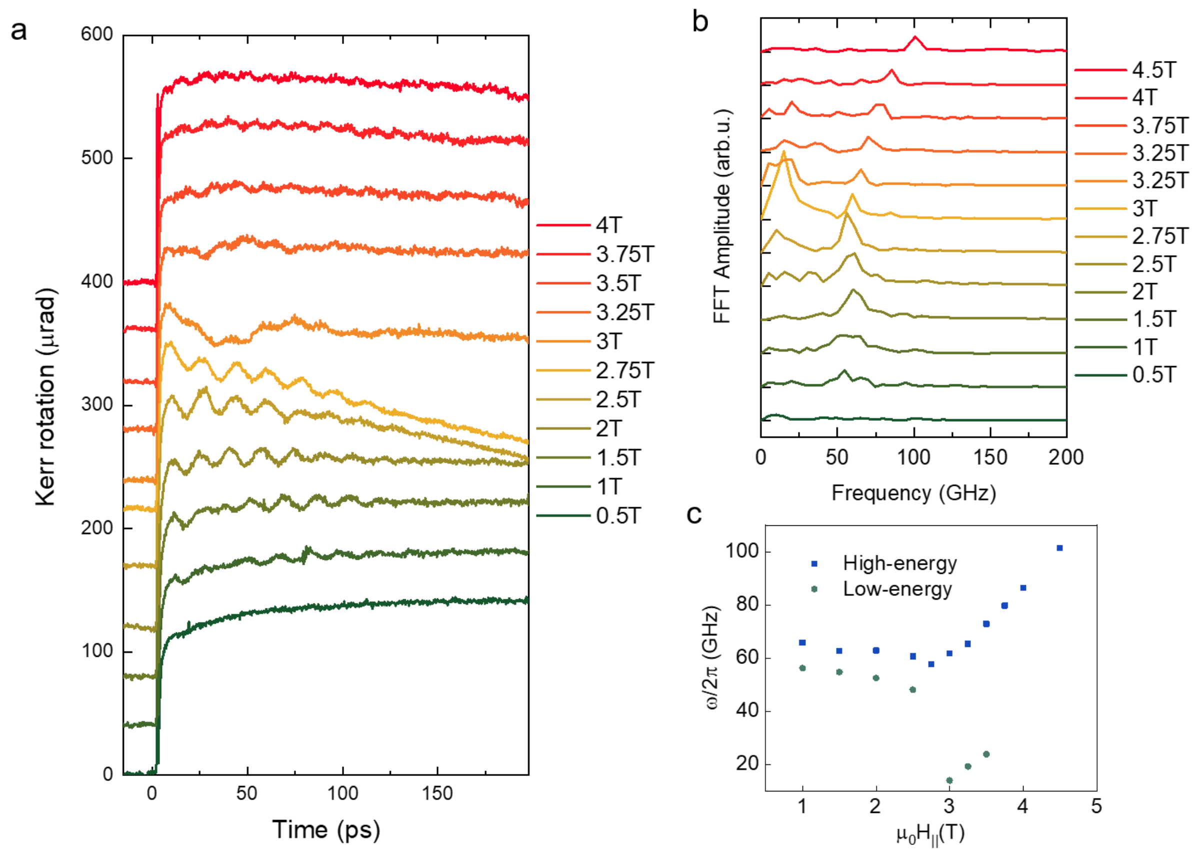

Figure S4 | Magnon oscillations at 25 K. a, Spin dynamics in bilayer CrI_3 under different in-plane magnetic fields. The curves are vertically displaced for clarity. **b,** Fast Fourier transform (FFT) amplitude spectra of **a. c,** In-plane field dispersion of the two magnon modes extracted from fitting the time-resolved MOKE signal with two harmonic oscillations.

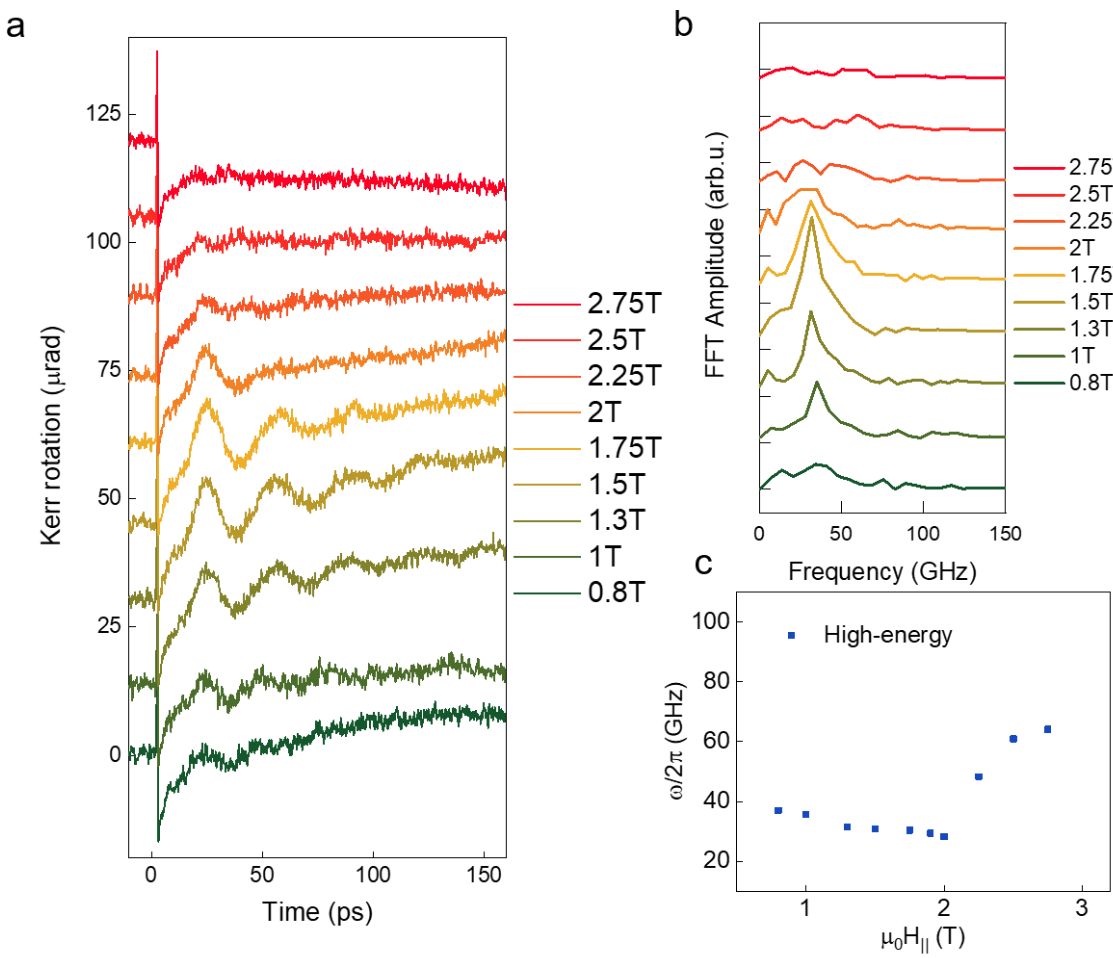

Figure S5 | Magnon oscillations at 45 K. Same as in Supplementary Fig. S4. Due to the weak signal, we can only identify the high-energy mode.

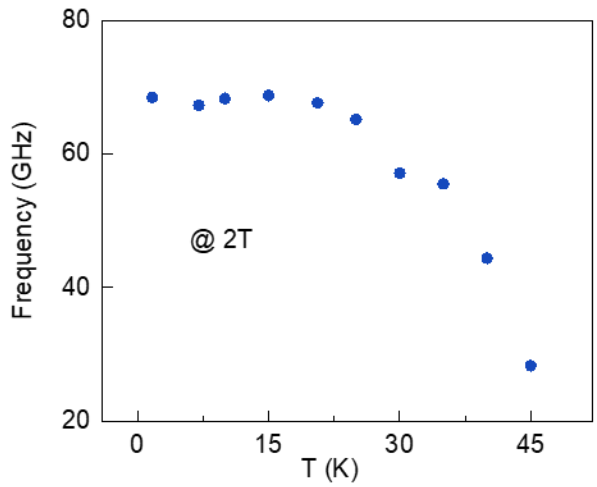

Figure S6 | Temperature dependence of the high-energy magnon mode under a fixed in-plane magnetic field of 2 T. All other experimental conditions are the same as in Fig. S4 and S5.

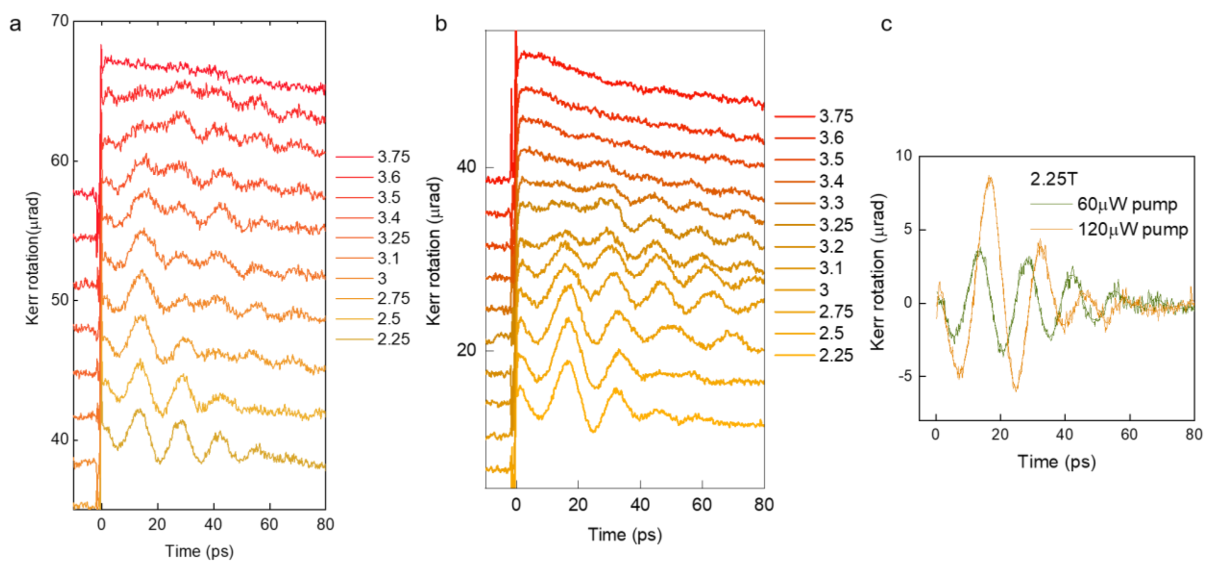

Figure S7 | Magnetic oscillations at different pump power. a,**b**, Time-resolved MOKE excited by pump power of 60 μW (**a**) and 120 μW (**b**) at 1.7 K. Measurements were performed under the same conditions. **c**, Direct comparison of oscillation traces under 2.25 T for the two pump powers. The amplitude of oscillations is proportional to the pump power. Frequency red shifts at higher pump power. The frequency shift can arise from a combined effect of elevated sample temperature and higher photo doping.

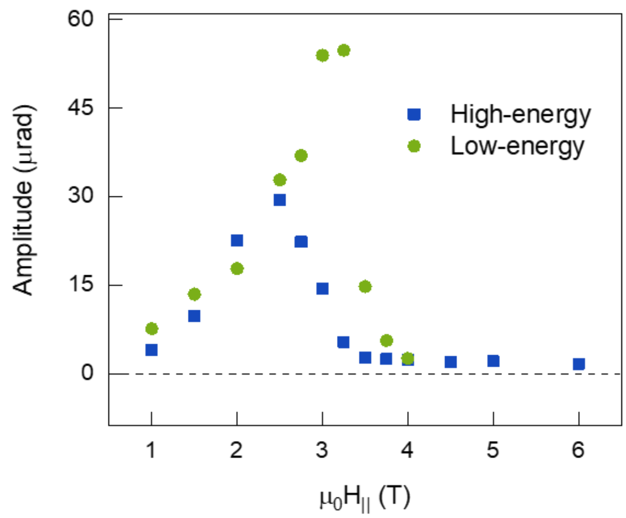

Figure S8 | Amplitude of the high-energy and low-energy modes extracted from the time-resolved MOKE (Fig. 2 of the main text).

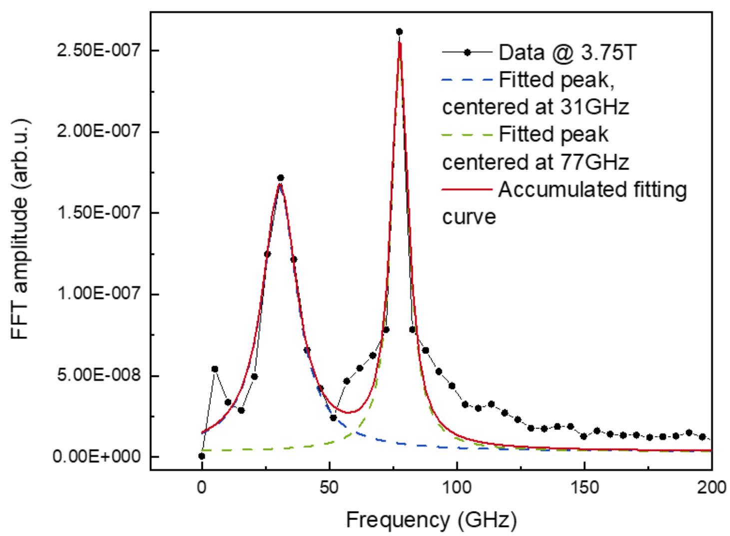

Figure S9 | FFT amplitude for the magnetic oscillations under an in-plane magnetic field of 3.75 T (symbols). The black line is a guide to the eye. The red line is the fit that includes two Voigt functions (dashed blue and green lines).

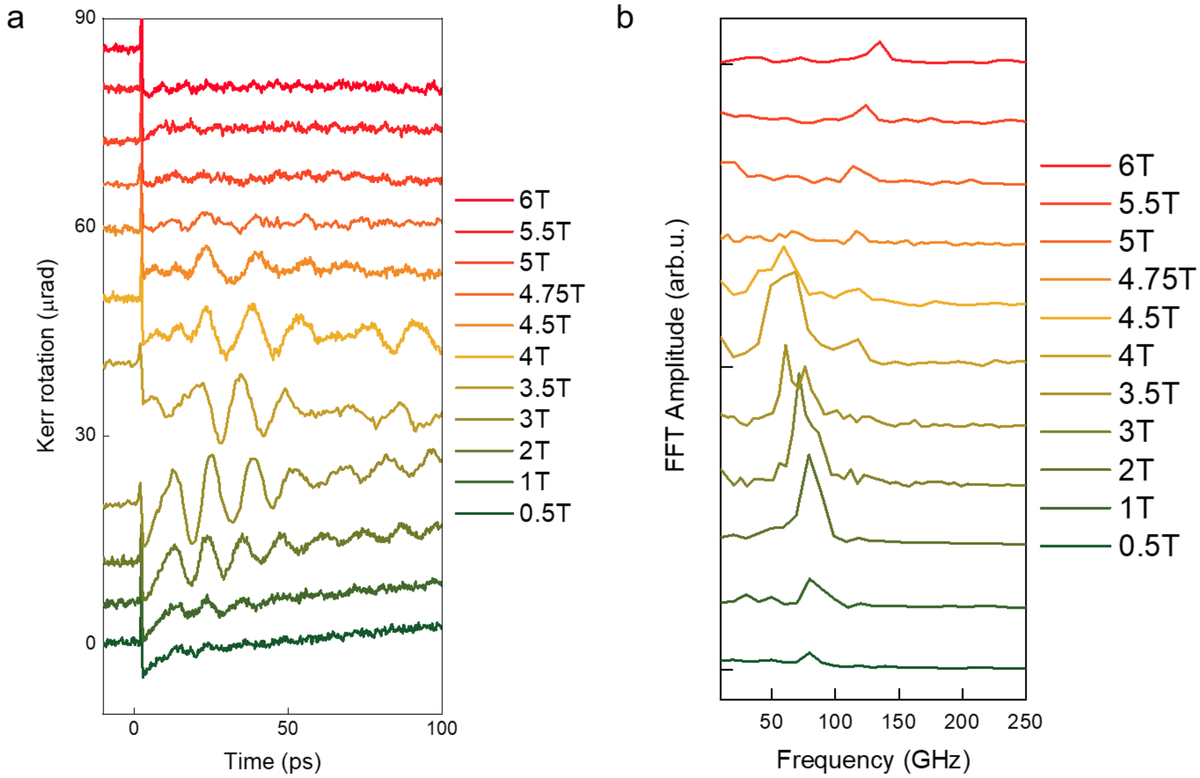

Figure S10 | Spin-wave dynamics in few-layer CrI_3 at 1.7 K. a, Time-resolved MOKE under different in-plane magnetic fields. **b,** FFT amplitude spectrum of **a**. The damping at 6 T is estimated to be ~ 0.04, which is similar to that in bilayer CrI_3.

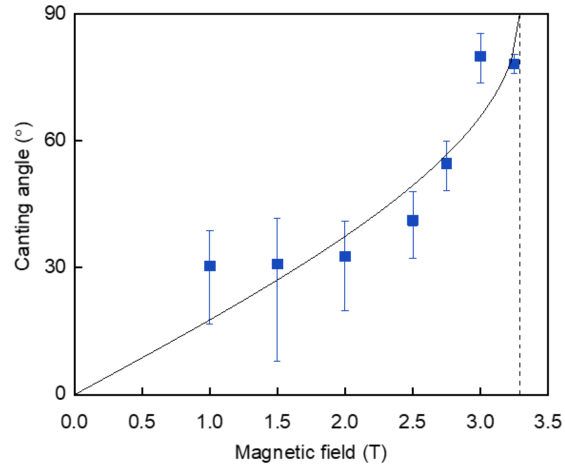

Figure S11 | Spin canting angle. Spin canting angle (with respect to the anisotropy axis) as a function of applied in-plane magnetic field. Symbols are evaluated from the mode frequencies of Fig. 3c and solid line represents $\theta = \sin^{-1}\left(\frac{H_{\parallel}}{H_S}\right)$ with $H_S \approx 3.3$ T. The dashed line marks the in-plane saturation field of ~3.3T.

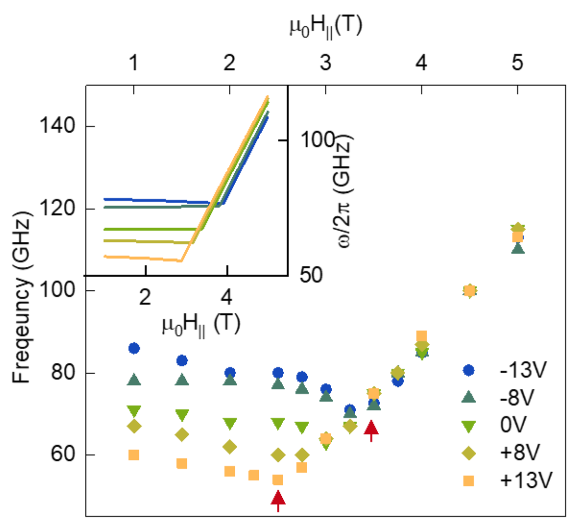

Figure S12 | Magnetic dispersion of spin-wave frequency at different gate voltages. The high-energy mode frequency are extracted as a function of magnetic field for the gate voltages measured in Fig. 4(a). The inset shows the corresponding fitting using LLG equations. The red arrows highlight the shift of in-plane saturation field, which is up to ~1T with the applied gate voltage.